Front. Earth Sci. 2018, 12(4): 693–710
https://doi.org/10.1007/s11707-018-0719-7

RESEARCH ARTICLE

Quantifying the early snowmelt event of 2015 in the Cascade Mountains, USA by developing and validating MODIS-based snowmelt timing maps

Donal O'LEARY III (✉)[1,2], Dorothy HALL[3,4], Michael MEDLER[2], Aquila FLOWER[2]

1 University of Maryland, Department of Geographical Sciences, College Park, MD 20740, USA
2 Western Washington University, Department of Environmental Studies, Bellingham, WA 98225, USA
3 National Aeronautics and Space Administration, Goddard Space Flight Center, Greenbelt, MD 20771, USA
4 Earth System Science Interdisciplinary Center, University of Maryland, College Park, MD 20740, USA

Abstract Spring snowmelt serves as the major hydrological contribution to many watersheds of the US West. Since the 1970s the conterminous western USA has seen an earlier arrival of spring snowmelt. The extremely low snowpack and early melt of 2015 in the Cascade Mountains may be a harbinger of winters to come, underscoring the interest in advancements in spring snowmelt monitoring. Target-of-opportunity and point measurements of snowmelt using meteorological stations or stream gauges are common sources of these data, however, there have been few attempts to identify snowmelt timing using remote sensing. In this study, we describe the creation of snowmelt timing maps (STMs) which identify the day of year that each pixel of a remotely sensed image transitions from "snow-covered" to "no snow" during the spring melt season, controlling for cloud coverage and ephemeral spring snow storms. Derived from the 500 m MODerate-resolution Imaging Spectroradiometer (MODIS) standard snow map, MOD10A2, this new dataset provides annual maps of snowmelt timing, with corresponding maps of cloud interference and interannual variability in snow coverage from 2001–2015. We first show that the STMs agree strongly with *in-situ* snow telemetry (SNOTEL) meteorological station measurements in terms of snowmelt timing. We then use the STMs to investigate the early snowmelt event of 2015 in the Cascade Mountains, USA, highlighting the protected areas of Mt. Rainier, Crater Lake, and Lassen Volcanic National Parks. In 2015 the Cascade Mountains experienced snowmelt 41 days earlier than the 2001–2015 average, with 25% of its land area melting > 65 days earlier than average. The upper elevations of the Cascade Mountains experienced the greatest snowmelt anomaly. Our results are relevant to land managers and biologists as they plan adaptation strategies for mitigating the effects of climate change throughout temperate mountains.

Keywords Cascade Mountains, snowmelt, spring, phenology, MODIS, remote sensing

Received September 15, 2017; accepted June 12, 2018

E-mail: donal@umd.edu

1 Introduction

Snow is a first-order control on ecosystems, influencing energy balance, hydrology, geomorphic processes, flora, and fauna (Billings and Bliss, 1959; Totland and Alatalo, 2002; Homan et al., 2011; Tahir et al., 2011; Moore et al., 2015). The US mountain west has seen an earlier arrival of spring weather since the 1970s, leading to snow melting 14–45 days earlier than average (Stewart, 2009), changes in plant phenology (Totland and Alatalo, 2002; Steltzer et al., 2009; Cornelius et al., 2013), altered water resource availability (Sproles et al., 2013), and a larger area burned by wildfires (Westerling et al., 2006; O'Leary III et al., 2016). Furthermore, model-based projections suggest that snowmelt may arrive an average of 10–40 days earlier across the continental US by the year 2100 (Stewart, 2009). The snow-dominated watersheds of the Cascade Mountains may be particularly vulnerable to climate change, as the mid-elevations of these mountains spend much of the winter near 0°C, and a change of only a few degrees could therefore alter the snowpack substantially (Nolin and Daly, 2006; Sproles et al., 2013) as an increase in freezing elevation level and possibility of rain-on-snow events deplete snowpack rapidly (McCabe et al., 2007). Perhaps as a harbinger of change, the years 2014 and

especially 2015, experienced an unusually low snow volume and early snowmelt in the Cascade Mountains (Margulis et al., 2016a; Sproles et al., 2017). Events like these and the widely-anticipated future reduction of snowpack and earlier arrival of spring snowmelt have created an increased interest in monitoring the timing of snowmelt.

While snowmelt timing is often defined as a single value for a watershed using streamflow (USGS, 2018) or measured in a single location at meteorological stations (NRCS, 2016), snowmelt timing is in reality a highly spatially heterogeneous process due to fine-scale variability in snow accumulation and spring heating patterns. Recent research has therefore started to explore the use of remotely sensed data to map snowmelt timing across the landscape as decreasing snow-covered area (Hall et al., 2012, 2015; O'Leary III et al., 2016; Nolin et al., 2017). Snowmelt timing has profound ecological implications at the landscape level (Billings and Bliss, 1959; Westerling et al., 2006; Inouye, 2008) and many snowmelt timing investigations have been motivated by questions of snow's control on ecological processes with the goal of providing a Day Of Year (DOY) for snowmelt timing to compare with similar DOY products for plant phenology (Jönsson and Eklundh, 2004; Zhang et al., 2006; Ganguly et al., 2010; Tahir et al., 2011). Previous attempts to define the timing of snow cover loss using optical remote sensing imagery have been largely unsuccessful due to cloud interference and validation issues (Narasimhan and Stow, 2010). However, studies from the wildfire literature have successfully identified the influence of snowmelt timing on annual area burned using cloud-free datasets (Semmens and Ramage, 2012; O'Leary III et al., 2016). With an increasing interest on climate's influence on plant phenology (University of Wyoming, 2017; Sherwood et al., 2017) and wildfire (Westerling, 2016), there is an obvious need for a gridded snowmelt timing dataset for use in ecological investigations (Littell et al., 2009; Abatzoglou and Kolden, 2013; O'Leary III et al., 2018).

In this paper we describe the development of annual Snowmelt Timing Maps (STMs) (O'Leary III et al., 2017), which identify the DOY that a given location becomes snow-free for the years 2001–2015, based on the Moderate Resolution Imaging Spectroradiometer (MODIS) Terra satellite standard snow-cover product MOD10A2 (Hall and Riggs, 2016; Riggs et al., 2017). We address the question: what was the spatial extent and temporal magnitude of the snowmelt timing anomaly of 2015 in the Cascade Mountains? In answering that question, we identify the areas having the greatest snowmelt timing anomaly in terms of their elevation, relative topography, and geographic location. We focus on the Cascade Mountains, and report specifically on results within three National Park Service (NPS) unit focus areas. Finally, we discuss the successes and limitations of this approach, with a particular focus on applications within the fields of hydrology, ecology, and land management.

2 Methods

The Cascade Mountains of the western conterminous US are part of a volcanic cordillera stretching from central Washington, through Oregon, and into northern California (Fig. 1). This region is known for its deep seasonal snowpack, expansive protected and recreational lands, and towering glacier-flanked volcanoes (USGS, 2014; NPS, 2016a). Here, we consider the Cascade Mountains along with case studies that focus on three National Park Service units: Mt Rainier (MORA), Crater Lake (CRLA), and Lassen Volcanic (LAVO) National Parks. These protected areas are the sites of active and long running ecological investigations and monitoring programs sponsored by federal agencies, non-profits, and academic institutions (NPS, 2016a, b, c). Additionally, these high-elevation areas are particularly vulnerable to climate change (Rangwala and Miller, 2012), and many at-risk species compete with invasive species for resources and survival (Wolf et al., 2016). Finally, these three study areas contain distinct environments offering a variety of snowmelt patterns– the massive glaciers of Mt Rainier contrasting with the subalpine meadows of Crater Lake, and the drier California climate of Mt Lassen volcano.

We developed the STMs (O'Leary III et al., 2017) spanning the area of North America, Greenland, and Iceland using a time-series analysis of the MOD10A2 Collection 5 data product (Hall et al., 2006). The MOD10A2 product is derived from a fractional snow cover product with the snow/no-snow threshold defined by 50% snow covered area. In this composite product, eight consecutive days of observations are compiled into a single image representing the 'maximum' snow cover for that period, with each pixel defined as snow-covered if snow was observed for one or more days during the composite period.

To define snowmelt timing, we recorded the DOY for the first snow-free image following snow cover, or a mixture of clouds and snow cover. To account for cloud-obscured MOD10A2 images we interpolated the dates between the last observed snow cover and the first observed snow-free date (Table 1). We recorded cloud interference as the number of consecutive 8-day composite images that were cloud-covered + 1. Pixels with more than four consecutive cloud-obscured images (32 days) between snow and no snow were omitted because of their poor validation results. We also calculated the count of STM values ('Count') identifying the number of years on record where the STM has a value (i.e., snow was present at some point that year, and snowmelt timing was successfully calculated). While late-season snowstorms

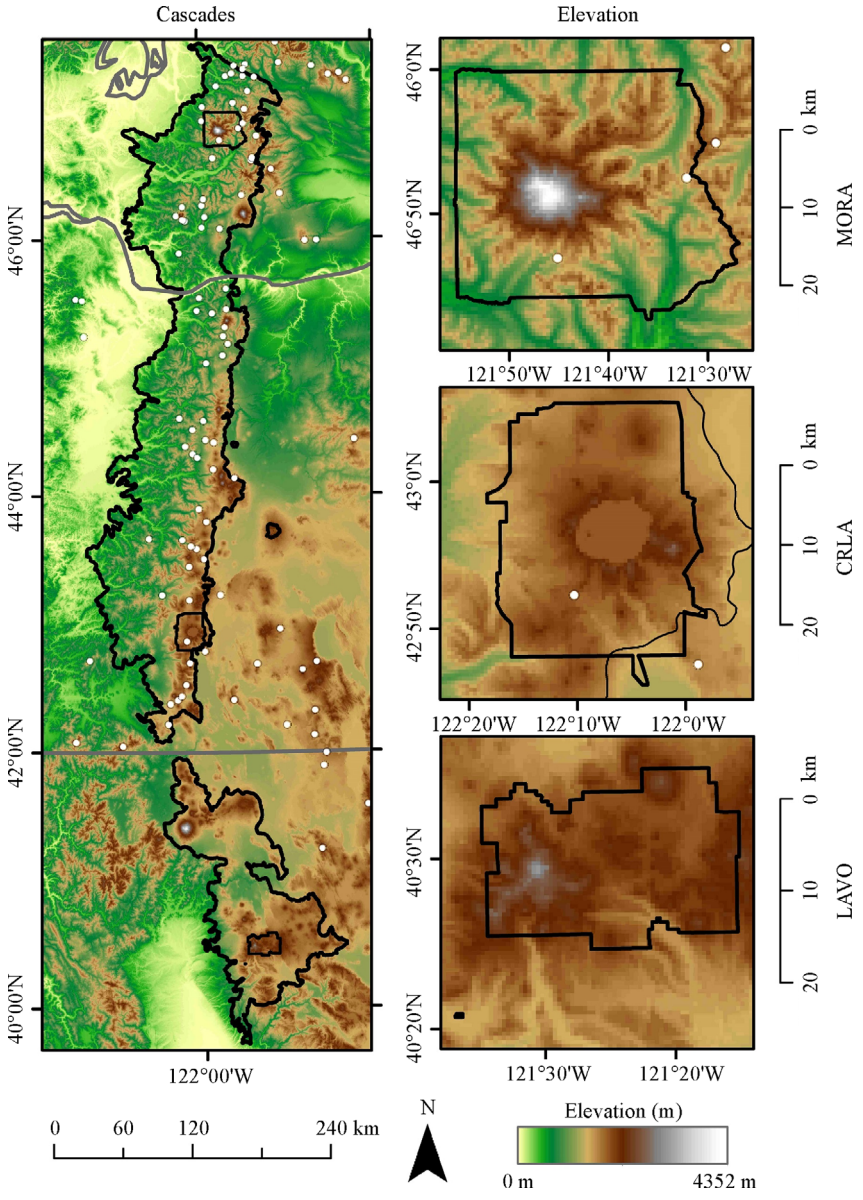

Fig. 1 Overview of study area elevation including Washington, Oregon, and California state boundaries (thick grey lines), the Cascade Mountains Ecoregion, and park unit polygons (thick black lines, left), and close-up views of Mt. Rainier (MORA), Crater Lake (CRLA) (with thin line of Cascade Mountains boundary visible crossing SE corner of the park), and Lassen Volcanic (LAVO) National Parks (right). SNOTEL stations are indicated by white circles with black outlines. Note that water bodies (including Crater Lake itself) are not differentiated on the elevation surface. Elevation data (30 m) resampled to resolution and registration of the STM data (500 m).

contribute appreciable water to the ecosystem, they are not the seasonal indicator and hydrologic input of the primary snowpack departure that we sought to capture in the STMs. To remove late-season snowstorms we disregarded any snow readings that occur following a 48-day period without snow (six consecutive 8-day composite images) beginning on February 26 or later. To validate our STMs, we compared the snowmelt timing values with the SNOw TELemetry (SNOTEL) station network spanning the western United States (NRCS, 2016) ($n = 854$). For a detailed explanation of STM development and validation see Appendix 1.

After validating against SNOTEL data, we divided our study area into four sections: the Cascade Mountains as a whole, and MORA, CRLA, and LAVO National Parks. We calculated Snow-Cover Depletion Curves (SCDCs) (Hall et al., 2015) for each region in software R version 3.2.3 by calculating the percentage of pixels (Y-axis) in each annual STM image with snowmelt DOY value greater than or equal to the daily time step (X-axis). The snowpack of the Cascade Mountains experiences substantially different dynamics at low, medium, and high elevations (Gleason et al., 2017), though comparing a particular elevation between the northern and southern extents of the Cascade

Table 1 Explanation of snowmelt and cloud interference logic for each pixel. Case describes the series of consecutive MOD10A2 image values. Snowmelt DOY is the resulting value in the STM. All DOY values are relative to the DOY of the no-snow MODIS image. Cloud interference values represent the number of temporally-interpolated images + 1, to avoid values of zero which may be confused as 'No Data' values in the STM dataset. For example, case 5 (bottom) shows a snow-covered composite image and a snow-free composite image separated by 4 consecutive images of no-snow. The resulting snowmelt value is interpolated to be the DOY of the snow-free image minus 16 (i.e., 32 days of separation between the snow- and no-snow images, divided by two), with a cloud interference value of 5 (4 cloud images, plus 1)

Case	Snowmelt DOY	Cloud Interference
Snow, Snow, No-Snow	DOY	1
Cloud, Snow, No-Snow	DOY	1
Snow, Cloud, No-Snow	DOY-4	2
Snow, Cloud, Cloud, No-Snow	DOY-8	3
Snow, Cloud, Cloud, Cloud, No-Snow	DOY-12	4
Snow, Cloud, Cloud, Cloud, Cloud, No-Snow	DOY-16	5

Mountains may find stark differences (e.g., at an elevation of 2000 m in MORA, one may encounter glaciers, while the same elevation may be hot, bare, and dry in LAVO). To capture these differences, we separated each study area into three elevation quantiles of equal area relative to the elevation range of each park (Table 2). We then found the mean snowmelt DOY for 2001–2015 and calculated the 2015 snowmelt anomaly for each area and elevation quantile.

3 Results

Validation results of snowmelt timing values between the STMs and SNOTEL stations reveals a high level of agreement. Differences between the STMs and all available SNOTEL stations have a mean error of 4.31 days. When we include only those stations within the Cascade Mountains we find a mean error of –4.76 days. These errors are less than the 8-day temporal resolution of the MOD10A2 product and therefore indicate that our STM algorithm captures on-the-ground snowmelt timing accurately. For a detailed description of this validation see Appendix 1.

The STMs show snowmelt timing gradually changing across the landscape, with low elevation areas and the arid lands to the east melting earlier than the land west of and including the crest of the Cascade Mountains (Fig. 2). When we investigate the 2015 snowmelt anomaly (relative to the 2001–2015 average), we find widespread earlier melt across the study area, with the vast majority of pixels experiencing a negative anomaly (Fig. 3). The average snowmelt timing anomaly was –41.45 days for the Cascade Mountains as a whole, and –32.94, –40.12, and –47.49 days for MORA, CRLA, and LAVO, respectively (Fig. 4, Table 3). Looking at the relative elevation of the Cascade Mountains as a whole, the lowest elevation areas experience less of an anomaly (–25.40 days) than do the middle (–45.05 days) and highest (–50.46 days) areas. This pattern is reversed for each national park, where the highest elevations experienced a lesser anomaly than the lower elevations within each park (Table 3). The year 2015 shows a generalized early melt, with much of the Cascade Mountains melting weeks to months earlier than the 15-year mean (Figs. 2 and 3). For the Cascade Mountains as a whole, and each national park studied here, there were locations where snowmelt timing occurred more than 100 days earlier than the 2001–2015 average (Fig. 3). 93.3% of the land area of the Cascade Mountains experienced an earlier than average snowmelt timing in 2015, along with 95.1% of MORA, 98.6% of CRLA, and 99.8% of LAVO. Ten percent of the land area of the Cascade Mountains had a snowmelt timing anomaly of $\geqslant$83.73 days earlier than average, and LAVO similarly had ten percent of its land area melt $\geqslant$80.53 or more days earlier than average. However, MORA and CRLA were somewhat insulated

Table 2 Pixel population sizes and elevation quantile limits for areas of interest (Q1 = lowest elevation, Q3 = highest)

Area	Sample size (n)	Elevation/m			
		Min	Q1 Max	Q2 Max	Q3 Max
Cascades	274118	2	883	1379	4352
MORA	4436	547	1320	1682	4352
CRLA	3420	1348	1770	1889	2675
LAVO	2016	1473	1995	2149	3106

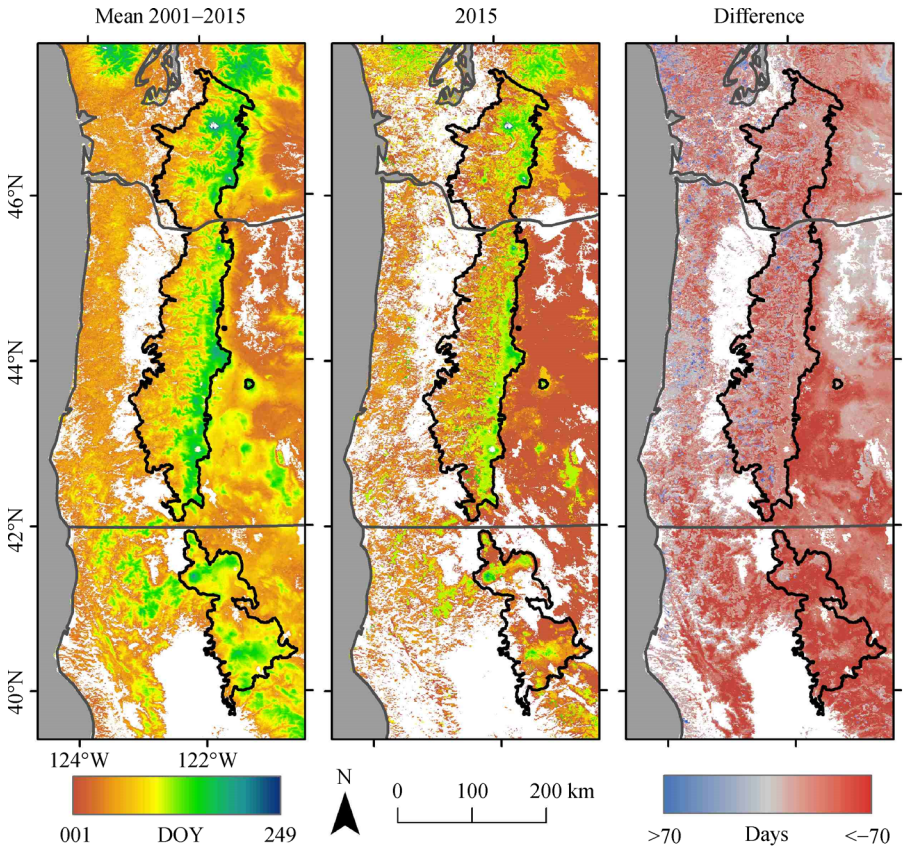

Fig. 2 Overview of STMs for the Cascade Mountains including outline of the Cascade Mountains Ecoregion (thick black line) and state boundaries (grey lines). Mean STM from 2001–2015, 2015 alone, and 2015-Mean difference are shown from left to right. White regions indicate areas with Count values less than 8 (mean) or no snow snowmelt detected (2015). Elevation quantile contour lines are omitted for clarity.

from the greatest anomaly magnitudes, with ten percent of their land area melting > 57 days earlier than average (Table 4).

The cloud interference output shows that the Cascade Mountains are subject to cloud interference during the snowmelt period (Fig. 5). In particular, cloud interference occurs most in the northern reaches, the low-elevation areas of the Columbia River gorge, and the western flanks of the Cascade Mountains crest. When we consider the number of years on record with a STM value, it is evident that the areas with the lowest Count of STM values often coincide with the highest cloud interference values (Fig. 5). While the mountainous areas of western Washington, Oregon, and northwestern California show high Count values approaching 15 years (i.e., they experience snow accumulation and snowmelt every year on record), the lower-elevation valleys and some parts of the central Oregon and the northeastern California altiplano show lower Count values, indicating an inconsistent inter-annual snowpack. Notably, MORA experiences high cloud interference values along with high Count values, suggesting that the snowmelt season is particularly cloudy at this location, leading to ambiguous detection of snowmelt timing. SCDCs for the Cascade Mountains and national parks show that in 2015 snow melts earlier than all other years throughout the melt season (Fig. 6). For each region 2015 has an earlier initial melt, earlier complete melt, and a lower SCA than all other years for the entire melt season (with the exception of LAVO melting out completely in 2001 several days earlier than in 2015).

4 Discussion

4.1 STMs and the 2015 snowmelt timing anomaly

The STM algorithm was successful in creating intuitive, ecologically sensible, and easy-to-employ maps for environmental analysis, which compare favourably with *in-situ* snow measurements. For large regions, visual inspection of the STMs is straightforward (Fig. 2), showing landscape patterns that relate to topography and regional climate. Viewing smaller areas (such as the national parks of interest, Fig. 4) we clearly see pixilation from the 500 m resolution of the MODIS snow-cover product. Still, subtle differences between elevations, slope

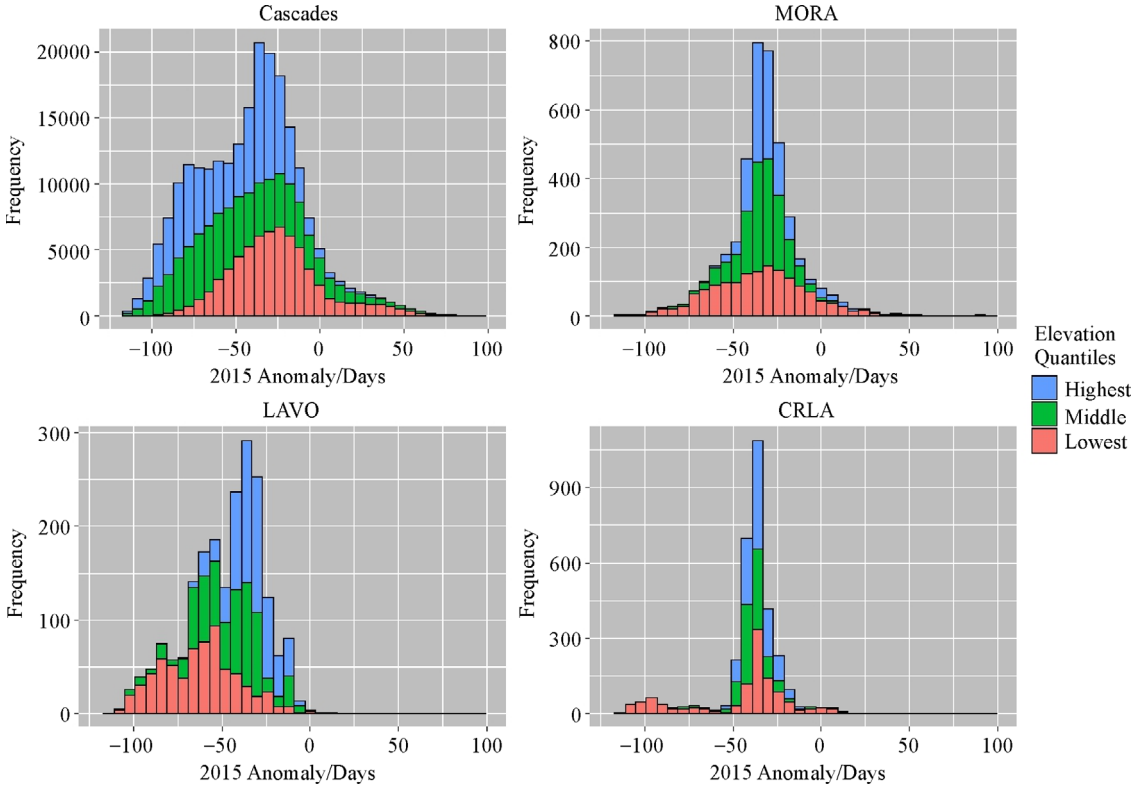

Fig. 3 2015 snowmelt anomaly distributions by study area (plot) and elevation quantile (color). Count describes the number of pixels with side length of ~500 meters. See Tables 2 and 3 for detailed statistics. Note how the Cascade Mountains as a whole experienced greater anomalies in the highest quantile (blue), while Mt. Rainier (MORA), Crater Lake (CRLA), and Lassen Volcanic (LAVO) National Parks experienced a greater anomaly in the lowest quantile (red).

gradients, and aspects highlight the landscape-level spatial heterogeneity of snowmelt and may yield insight for land managers or other stakeholders.

The year 2015 had a widespread early snowmelt event across the Cascade Mountains. Our SCDCs show that 2015 had substantially lower snow-covered area than all other years on record for the Cascade Mountains as a whole and each national park of interest (Fig. 6). These results are consistent with other analyses of the 2015 snow year throughout the Cascade and Sierra Nevada ranges (Margulis et al., 2016a, b; Sproles et al., 2017). Compared with the spatial mean of snowmelt DOY values, we see that the 2015 early snowmelt event was widespread, though non-uniform, throughout the study area. Stratifying study areas by elevation we see that for the Cascade Mountains as a whole, the high elevations had the greatest anomaly (Table 3). However, the individual parks are much higher in elevation, with LAVO existing completely within the Cascade Mountains highest quantile. When we look at the quantiles within these smaller study areas we see that the lowest elevations experienced the greatest anomalies (LAVO Q1 is particularly devastated at –62.35 days), while the highest elevations experienced the smallest anomalies within the parks (~ –30 days) (Fig. 3, Table 3). Some high-elevation mountain ecosystems experience greater warming than the global average (Rangwala and Miller, 2012), and while we see this effect when looking at the Cascade Mountains as a whole, our results show that the highest elevation areas within the national parks experienced less of a snowmelt anomaly than the lower-elevation slopes surrounding the volcanoes (Table 3). This may be driven by many different factors, including land cover, stochastic weather events, and vegetation. Forest composition influences snowpack dynamics by changing canopy interception and radiation balance, and forested and non-forested areas retain and ablate snow in different ways (Roth and Nolin, 2017), though it is unclear how these forces have contributed to this event of 2015. Perhaps the areas near treeline experience the greatest anomaly because they are typically slightly below freezing, needing an increase of only a few °C to cause major snowmelt timing changes, while the highest elevations were still well below freezing for much of the melt season (Mote et al., 2005). While there is no single driver of the elevational pattern that we see in our results, further investigations may consider these elements when isolating snowmelt events in particular locations.

Cloud cover occasionally prevents an ideal snowmelt detection, leading to a temporally interpolated snowmelt DOY value (Table 1, Case 3 +), and a reduced temporal

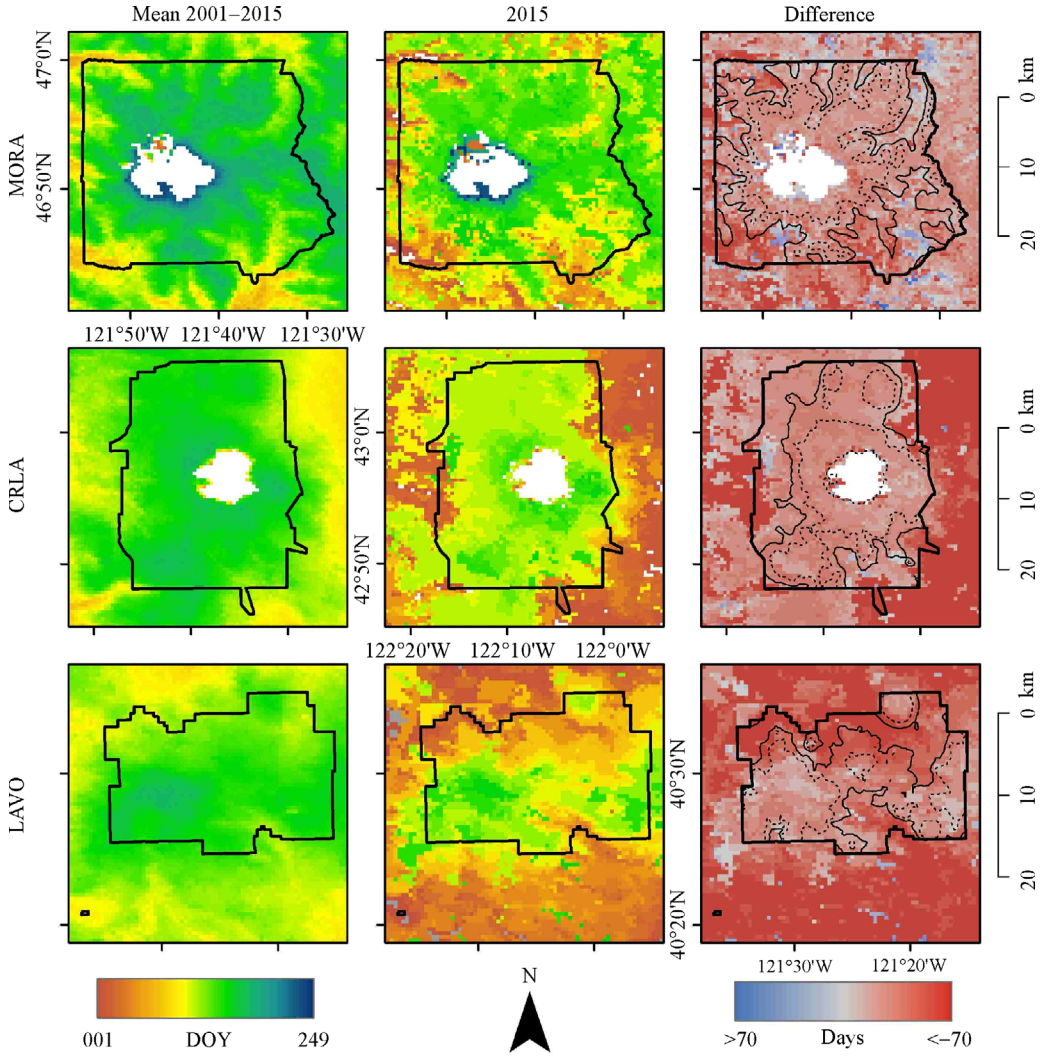

Fig. 4 Maps of Mt. Rainier (MORA), Crater Lake (CRLA), and Lassen Volcanic (LAVO) National Parks (top to bottom), showing 2001–2015 mean STM, 2015 STM, and 2015-mean difference (left to right). In the difference panels, the thin solid black line indicates the lower bound of the middle elevation quantile, and the dashed line indicates the lower bound of the upper elevation quantile (Table 2). The year 2015 shows early snowmelt for most of each park, however the lower-elevation areas surrounding the volcanoes show a greater difference than the high-elevation areas within the parks. White regions indicate areas with Count values less than 8 (mean) or no snow snowmelt detected for the year 2015, primarily located in the glaciers of MORA, and Crater Lake itself.

Table 3 Descriptive statistics for distributions of anomalies by study area and elevation quantile (Q1 = lowest elevation, Q3 = highest). Mean snowmelt timing includes years 2001–2015 and excludes points with fewer than 8 years of coverage. 2015 anomaly is calculated on a per-pixel basis by subtracting the mean from the year 2015

Area	Mean snowmelt timing (DOY)				Snowmelt timing standard deviation				2015 Mean anomaly (Days)				2015 anomaly standard deviation			
	Full	Q1	Q2	Q3	Full	Q1	Q2	Q3	Full	Q1	Q2	Q3	Full	Q1	Q2	Q3
Cascades	94.86	60.63	96.59	127.42	37.58	19.62	28.16	28.72	–41.45	–25.40	–45.05	–50.46	31.91	28.48	33.87	27.9
MORA	154.21	128.88	159.83	175.83	31.66	20.55	13.4	36.54	–32.94	–35.46	–33.90	–28.74	20.58	26.63	13.88	18.27
CRLA	147.75	137.58	145.28	160.14	18.38	12.28	23.67	8.2	–40.12	–46.12	–38.07	–35.76	19.38	28.93	10.81	8.2
LAVO	141.76	128.43	142.49	154.37	15.32	11.42	9.7	11.92	–47.49	–62.35	–46.29	–33.88	21.45	21.8	18.83	12.03

Table 4 Snowmelt timing quantiles for the Cascade Mountains and Mount Rainier, Crater Lake, and Lassen Volcanic National Parks. The values shown here describe 2015 snowmelt timing anomaly experienced by a given percentage of land area for each study area in days. For example, 10% of the land area for the Cascade Mountains had a snowmelt timing anomaly of ⩾83.73 days earlier than the 2001–2015 average

Area	2015 snowmelt timing anomaly percentile (days)				
	10%	25%	50%	75%	90%
Cascades	–83.73	–65.60	–39.20	–21.87	–4.27
MORA	–57.60	–41.60	–32.80	–24.27	–10.93
CRLA	–57.01	–42.13	–37.33	–32.00	–24.00
LAVO	–80.53	–60.80	–43.20	–32.00	–23.28

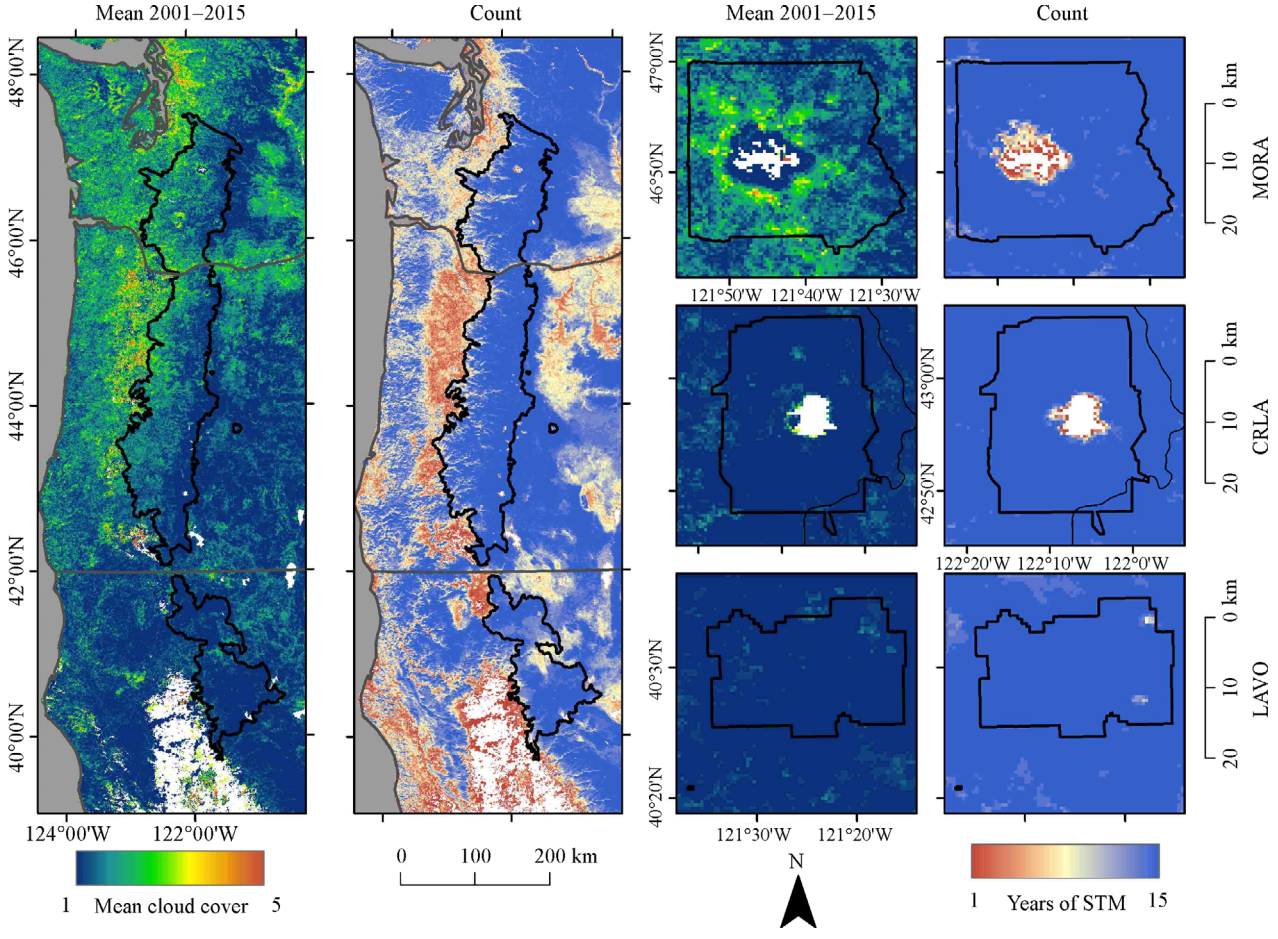

Fig. 5 Cloud Interference and Count maps for the Cascade Mountains and national parks of interest. Mean cloud cover maps show the mean cloud interference values per pixel from 2001–2015, as described in Table 1. Count maps show the number of years of STM coverage, with mountainous regions experiencing accumulation and observable snowmelt for most, if not all, of the 15 years on record (darkest blue, 'Count' images). Note that mean cloud interference values disregard null values (years without STM values) and may therefore overestimate mean cloud interference for regions with low Count values. White areas (MORA glaciers, Crater Lake itself, Northern California valleys) have no snow observations for the period record.

precision. In our validation, increasing cloud cover corresponded with greater errors between the STMs and SNOTEL stations, with the STMs estimating a later date of snow loss than the SNOTEL stations (Appendix 1). Generally, cloud interference is greater in the northern end of the Cascade Mountains, as Washington State, and MORA in particular, show higher cloud interference values than the Oregon and California parts of the ecoregion (Fig. 5). Throughout the range, cloud cover is also greater along the western foothills, owing to the orographic cloud formation and precipitation driven by the uplift of the Cascade Mountains. Predominant weather patterns direct humid coastal air from west to east, which frequently forms clouds on the western side of the

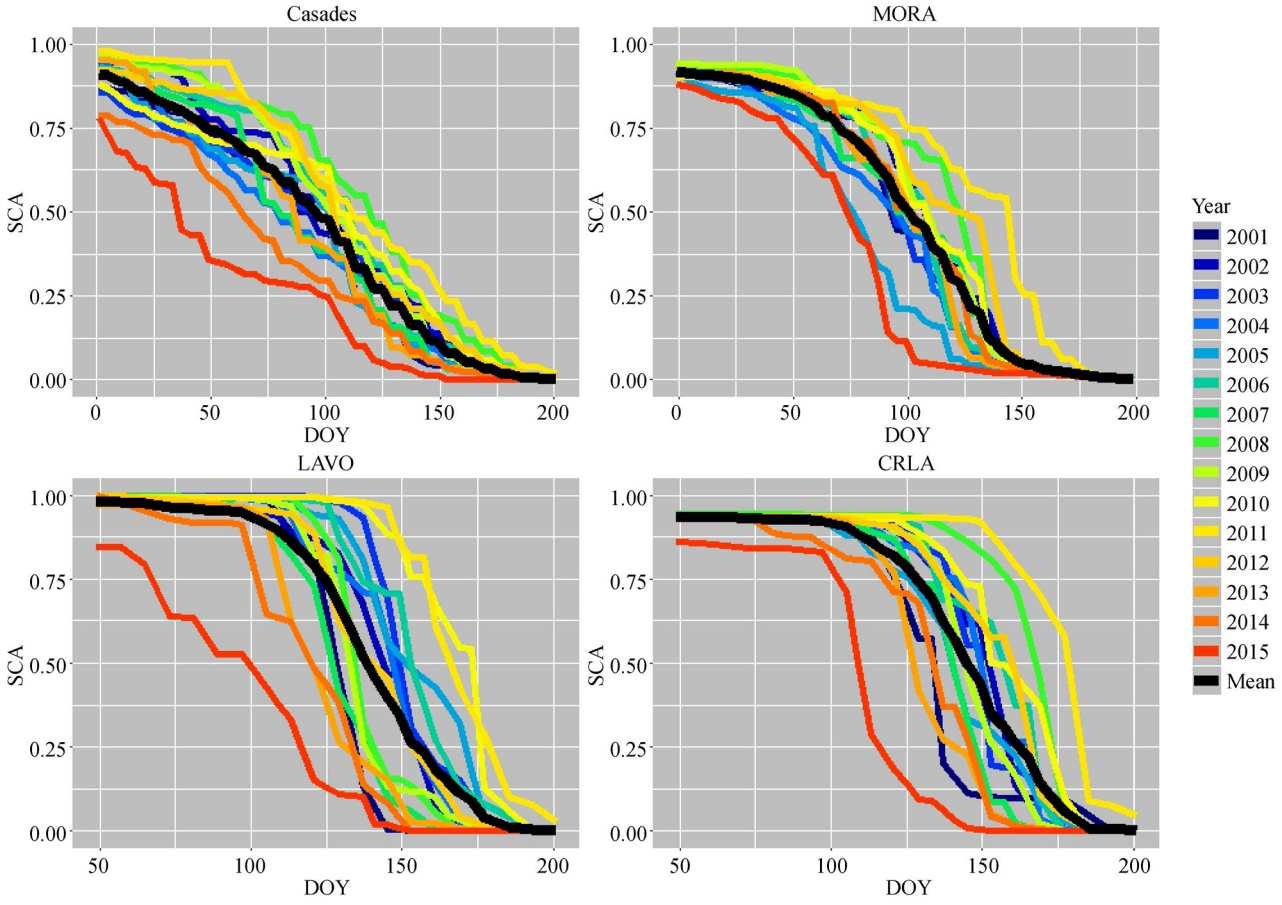

Fig. 6 Snow-cover depletion curves (SCDCs) for the Cascade Mountains, MORA, CRLA, and LAVO. Mean SCDC is calculated as the mean (black) of all SCDCs from 2001–2015, not from the mean STM image. The year 2015 (red) is clearly the earliest melt of all years for all regions, with an earlier initial melt and earlier complete melt than all other years. Note that each *X*-axis is focused on melt season for each region.

mountains as topography-driven uplift causes rapid cooling and precipitation. This also creates a well-known "rain shadow" east of the Cascade Mountains where sunny, dry days are common. Ultimately, the patterns shown in Fig. 5 are sensible and expected for this ecoregion.

There are many areas that experience snow cover for some, but not all, years on record (Fig. 5). Many of the low-elevation valleys on the western flanks of the Cascade Mountains, as well as the low-elevation areas separating LAVO from the rest of the Cascade Mountains, have a Count value less than 15. We calculated the mean cloud interference values by ignoring years without a snowmelt value, so within areas that have low Count values a single year with a high cloud interference value may result in a higher mean cloud interference value than an area with 15 years of coverage. Keeping this effect in mind, we see the areas within Fig. 5 with a low Count often have a high mean cloud interference value, particularly within the Puget Sound and Willamette Valley. Interestingly, within the Columbia River Valley we see a high Count value with a high cloud interference value, likely owing to persistent fog and low clouds that funnel into the Columbia River Valley from the Pacific coast during the melt season. For our visualizations we mask pixels with Count values less than 8 to highlight regions with a consistent perceptible snowmelt ($>$ 50% occurrence).

4.2 Limitations

There are numerous limitations involved in the application of our STMs. Of primary concern is the 8-day resolution of this product. While the MOD10A2 does improve upon the MOD10A1 daily product in terms of cloud-free data, it is still limited by some cloud cover, its 8-day resolution, and inherent snow reporting biases (Hall and Riggs, 2007). This 8-day resolution differs from the daily or hourly resolution available using meteorological stations (SNOTEL) and limits the precision of any snowmelt observation to eight days. Still, when investigating large areas, particularly if averaging snowmelt DOY values, this fairly coarse temporal resolution is smoothed by the many points available from the moderate spatial resolution, and the 8-

day composites streamline data processing compared to daily resolution products. Alternative snow datasets are available, though they have their own limitations. The SNOw Data Assimilation System (SNODAS) offers 1 km snow products including extent, SWE, temperature, and more, from late 2003–present (Barrett, 2003). This product is limited by its methods for this kind of application (computer modelled from several *in-situ* and remotely-sensed inputs), and therefore likely has a reduced accuracy at the margins of snow cover compared to the MOD10 products. The widely-employed Ice Mapping System (IMS) (Ramsay, 1998) is also derived from multiple inputs, though spatial resolution for the time period of this study is poor at 24 km, for the earlier part of our study period, with the 4 km and 1 km resolution IMS products becoming available more recently. Further research should employ the cloud-gap-filled daily MOD10A1F product in Version 6 (Hall and Riggs, 2016), though this would require a non-trivial revision of the Python scripts used for the snowmelt timing algorithm, and substantially increase storage and computational demand. These methods will also be robust in the future using the Visible Infrared Imaging Radiometer Suite (VIIRS) (Riggs et al., 2017).

When looking closely at the national parks of interest we see areas with low Count values around the glaciers of MORA, and the seasonal lake ice of CRLA. In MORA, some years show extensive snowmelt, and possibly glacier retreat, exposing crags and rocky slabs that are typically snow and ice covered throughout the year. This leads to snowmelt values in locations that do not usually experience snowmelt, resulting in a low Count values on and around this volcano's glaciers. These areas also experience extensive cloud cover for much of the year, also leading to low Count values. The possible signal from glacier retreat should not be confounded with high cloud interference, and deserves further investigation, though we recommend the use of higher spatial resolution products for glacier monitoring in temperate regions. CRLA experiences different lake ice extents depending on the winter. When this lake ice is snow-covered it is classified as snow in the MOD10A2 data product, leading to snowmelt timing values where there typically are none. These effects lead to subtle changes in the SCA by increasing the total snow-covered area of the study site (Fig. 6), and may be of interest for particular applications, though for our purposes these data points have little influence on the bigger picture in terms of ecology and hydrology.

Validating the STMs with SNOTEL measurements is useful, though the differences between the data collections methods complicate their comparison. Cloud interference is not a problem for SNOTEL locations, as SWE observations are collected using a pressure transducer. This difference may lead to snowmelt timing disagreement where the STM for that year is cloud-interfered. SNOTEL locations are reported by latitude and longitude to the hundredth of a decimal degree, and this low spatial precision may lead to registration mismatch between SNOTEL location and the STM pixel that it exists within. Additionally, the forest (or lack thereof) surrounding any SNOTEL station may influence this reading as different forest types have substantially different interception and radiation properties (Lundquist et al., 2013; Dickerson-Lange et al., 2017; Roth and Nolin, 2017). Finally, the 30 cm SWE threshold may not be appropriate for all ecosystems and years, and adjusting this value may improve the comparison results (Appendix 1).

4.3 Further investigation

Continued development of the snowmelt detection algorithm will yield further insight into quantifying snowmelt timing. The STMs are currently limited to an 8-day resolution stemming from the MOD10A2 parent data. Creating new STMs using the Collection 006 cloud-gap-filled product, MOD10A1F, could improve temporal resolution, possibly improving the SNOTEL comparison and delivering a higher temporal precision. Improving explicit reporting of details such as cloud coverage and late-season snow events may benefit certain users who demand specific criteria for ecological modelling. Expanding the spatial domain of this dataset into a global data product would be a substantial improvement but would require experts from around the world for validation and harmonization with local snow cycles. Research into the specific meteorological conditions leading up to and including the snowmelt season of 2015, including air temperature and Pacific Ocean surface temperature anomalies, could help to pair some of the anomaly characteristics with particular weather events such as shifts in freezing level or precipitation. This would be particularly insightful to explore why the low elevations of the national parks experienced the greatest anomalies. Finally, collaboration with researchers in many fields will yield insights into improvements that would benefit further iterations of the STMs. These STMs have been found to have significant relationships with plant phenology data based on the normalized-difference vegetation index, within CRLA (O'Leary III et al., 2018) and similar snowmelt timing maps are known to have ecologically significant relationships with wildfire (Semmens and Ramage, 2012; O'Leary III et al., 2016), demonstrating that many other ecological questions can be addressed using the STMs.

5 Conclusions

We developed an algorithm for time series analysis of the MOD10A2 MODIS snow-cover data product and used this algorithm to quantify snowmelt timing and create snowmelt timing maps (STMs) for North America from

2001–2015 (O'Leary III et al., 2017). We validated the STMs against *in-situ* SNOTEL stations located throughout the western United States including Alaska, which proved to have strong agreement (Appendix 1). The derived snowmelt timing values follow topography, with elevation, slope, and aspect all contributing to spatial heterogeneity. Comparing snow years from 2001–2015 we present snow-cover depletion curves (SCDCs) for the Cascade Mountains as a whole, and for Mt Rainier, Crater Lake, and Lassen Volcanic National Parks individually, and identify spatial and temporal snowmelt trends.

Within the 2001–2015 study period, the year 2015 experienced the earliest initial melt, the earliest complete melt, and the lowest snow-covered area throughout the entire melt period for each region of interest, with a single exception (Fig. 6). The 2015 snowmelt averaged 41.45 days earlier snowmelt in the Cascade Mountains as a whole, with the highest elevations having the greatest snowmelt timing anomaly. Interestingly, the national parks in isolation had the largest snowmelt anomaly at their lowest elevations, suggesting that this mountain range is particularly vulnerable to early snowmelt events near and below treeline. Our new method of quantifying snowmelt timing is especially useful to identify locations where seasonal snowpack is highly sensitive to changes in climate, such as the Cascade Mountains (Nolin and Daly, 2006; Sproles et al., 2013). These results are relevant in hydrology (Musselman et al., 2017), cryosciences, earth energy balance, and phenology (Sherwood et al., 2017; O'Leary III et al., 2018), as well as to land managers, and the general public as they keep a close eye on snowpack dynamics of the Cascade Mountains and other lands for the decades to come.

Code and data availability

Code in Python and R for the snowmelt timing development and quantitative analysis are available from the corresponding author. Snowmelt Timing Maps including cloud interference, count, and mean calculations for 2001–2015 are available from the Oak Ridge National Laboratory, USA. https://doi.org/10.3334/ORNLDAAC/1504

Acknowledgements This material is based upon work supported by the National Science Foundation Graduate Research Fellowship Program under Grant No. DGE1322106. Co-author Hall was funded through NASA grant 80NSSC17K0172. Any opinions, findings, and conclusions or recommendations expressed in this material are those of the authors and do not necessarily reflect the views of the National Science Foundation. We thank Dr. Jherime Kellermann, Chris Wayne, Crater Lake National Park, the University of Washington, and the George Melendez Wright Foundation for supporting the Young Leaders in Climate Change program, during which D. O'Leary III developed earlier iterations of the STMs. We also thank Dr. Christopher Crawford, Dr. Andrew Bunn, and Dr. David Wallin for their suggestions in refining the STMs.

References

Abatzoglou J T, Kolden C A (2013). Relationships between climate and macroscale area burned in the western United States. Int J Wildland Fire, 22(7): 1003–1020

Barrett A (2003). National Operational Hydrologic Remote Sensing Center SNOw Data Assimilation System (SNODAS) Products at National Snow and Ice Data Center. Special Report #11https://nsidc.org/sites/nsidc.org/files/files/nsidc_special_report_11.pdf

Billings W D, Bliss L C (1959). An alpine snowbank environment and its effects on vegetation, plant development, and productivity. Ecology, 40(3): 388–397

Brown R D, Brasnett B, Robinson D (2003). Gridded North American monthly snow depth and snow water equivalent for GCM evaluation. Atmos-ocean, 41(1): 1–14

Brubaker K L, Pinker R T, Deviatova E (2005). Evaluation and comparison of MODIS and IMS snow-cover estimates for the continental United States using station data. J Hydrometeorol, 6(6): 1002–1017

Cornelius C, Leingärtner A, Hoiss B, Krauss J, Steffan-Dewenter I, Menzel A (2013). Phenological response of grassland species to manipulative snowmelt and drought along an altitudinal gradient. J Exp Bot, 64(1): 241–251

Crawford C J (2014). MODIS Terra Collection 6 fractional snow cover validation in mountainous terrain during spring snowmelt using Landsat TM and ETM+. Hydrol Processes, 29(1): 128–138

Dickerson-Lange S E, Gersonde R F, Hubbart J A, Link T E, Nolin A W, Perry G H, Roth T R, Wayand N E, Lundquist J D (2017). Snow disappearance timing is dominated by forest effects on snow accumulation in warm winter climates of the Pacific Northwest, United States. Hydrol Processes, 31(10): 1846–1862

Fassnacht S R, Sexstone G A, Kashipazha A H, López-Moreno J I, Jasinski M F, Kampf S K, Von Thaden B C (2016). Deriving snow-cover depletion curves for different spatial scales from remote sensing and snow telemetry data. Hydrol Processes, 30(11): 1708–1717

Ganguly S, Friedl M A, Tan B, Zhang X, Verma M (2010). Land surface phenology from MODIS: characterization of the Collection 5 global land cover dynamics product. Remote Sens Environ, 114(8): 1805–1816

Gleason K E, Nolin A W, Roth T R (2017). Developing a representative snow-monitoring network in a forested mountain watershed. Hydrol Earth Syst Sci, 21(2): 1137–1147

Hall D K, Crawford C J, DiGirolamo N E, Riggs G A, Foster J L (2015). Detection of earlier snowmelt in the Wind River Range, Wyoming, using Landsat imagery, 1972–2013. Remote Sens Environ, 162(1): 45–54

Hall D K, Foster J L, DiGirolamo N E,Riggs G A (2012). Snow cover, snowmelt timing, and stream power in the Wind River Range, Wyoming. Geomorphology, 137(1): 87–93

Hall D K, Riggs G A (2007). Accuracy assessment of the MODIS snow products. Hydrol Processes, 21(12): 1534–1547

Hall D K, Riggs G A (2016). MODIS/Terra Snow Cover Daily L3 Global 500 m Grid, Version 6. NASA National Snow and Ice Data Center Distributed Active Archive Cente https://doi.org/10.5067/

MODIS/MOD10A1.006

Hall D K, Salomonson V V, Riggs G A (2006). MODIS/Terra Snow Cover 8-Day L3 Global 500m Grid. Version 5. National Snow and Ice Data Center

Homan J W, Luce C H, McNamara J P, Glenn N F (2011). Improvement of distributed snowmelt energy balance modeling with MODIS-based NDSI-derived fractional snow-covered area data. Hydrol Processes, 25(4): 650–660

Inouye D W (2008). Effects of climate change on phenology, frost damage, and floral abundance of Montane Wildflowers. Ecology, 89 (2): 353–362

Inouye D W, Morales M A, Dodge G J (2002). Variation in timing and abundance of flowering by Delphinium barbeyi Huth (Ranunculaceae): the roles of snowpack, frost, and La Niña, in the context of climate change. Oecologia, 130(4): 543–550

Iorio J P, Duffy P B, Govindasamy B, Thompson S L, Khairoutdinov M, Randall D (2004). Effects of model resolution and subgrid-scale physics on the simulation of precipitation in the continental United States. Clim Dyn, 23(3–4): 243–258

Jönsson P, Eklundh L (2004). TIMESAT– a program for analysing time-series of satellite sensor data. Comput Geosci, 30(8): 833–845

Klein A G, Barnett A C (2003). Validation of daily MODIS snow cover maps of the Upper Rio Grande River Basin for the 2000–2001 snow year. Remote Sens Environ, 86(2): 162–176

Littell J S, McKenzie D, Peterson D L, Westerling A L (2009). Climate and wildfire area burned in western U.S. ecoprovinces, 1916—2003. Ecol Appl, 19(4): 1003–1021

Lundquist J D, Dickerson-Lange S E, Lutz J A, Cristea N C (2013). Lower forest density enhances snow retention in regions with warmer winters: a global framework developed from plot-scale observations and modeling. Water Resour Res, 49(10): 6356–6370

Margulis S A, Cortés G, Girotto M, Durand M (2016b). A Landsat-Era Sierra Nevada snow reanalysis (1985–2015). J Hydrometeorol, 17 (4): 1203–1221

Margulis SA, Cortés G, Girotto M, Huning LS, Li D, Durand M (2016a). Characterizing the extreme 2015 snowpack deficit in the Sierra Nevada (USA) and the implications for drought recovery. Geophysical Research Letters, 43(12): 2016GL068520

McCabe G J, ClarkM P, Hay L E (2007). Rain-on-snow events in the western United States. Bull Am Meteorol Soc, 88(3): 319–328

Moore C, Kampf S, Stone B, Richer E (2015). A GIS-based method for defining snow zones: application to the western United States. Geocarto Int, 30(1): 62–81

Mote P W, Hamlet A F, Clark M P, Lettenmaier D P (2005). Declining mountain snowpack in western North America. Bull Am Meteorol Soc, 86(1): 39–49

Musselman K N, Molotch N P, Margulis S A (2017). Snowmelt response to simulated warming across a large elevation gradient, southern Sierra Nevada, California. Cryosphere, 11(6): 2847–2866

Narasimhan R, Stow D (2010). Daily MODIS products for analyzing early season vegetation dynamics across the North Slope of Alaska. Remote Sens Environ, 114(6): 1251–1262

Nolin A W, Daly C (2006). Mapping “At Risk” Snow in the Pacific Northwest. J Hydrometeorol, 7(5): 1164–1171

Nolin A W, Sproles E A, Crumley R L, Wilson A, Mar E, van de Kerk M, Prugh L (2017). Cloud-based Computing and Applications of New Snow Metrics for Societal Benefit. AGU Fall Meeting Abstracts, 22

NPS (2016a). Science and Learning Center. http://www.nps.gov/crla/slc.htm. Accessed 7 Mar 2016

NPS (2016b). Ongoing and Past Research. http://www.nps.gov/mora/learn/nature/past-research.htm. Accessed 7 Mar 2016

NPS (2016c). Klamath Network Inventory and Monitoring. http://science.nature.nps.gov/im/units/klmn/. Accessed 7 Mar 2016

NRCS (2016). NRCS National Water and Climate Center | SNOTEL Data & Products. http://www.wcc.nrcs.usda.gov/snow/. Accessed 3 Sep 2016

O’Leary III D S, Bloom T D, Smith J C, Zempf C R, Medler M J (2016). A new method comparing snowmelt timing with annual area burned. Fire Ecol, 12(1): 41–51

O’Leary III D S, Hall D K, Medler M J, Matthews R A, Flower A (2017). Snowmelt Timing Maps Derived from MODIS for North America, 2001–2015. Oak Ridge National Laboratory. https://doi.org/10.3334/ORNLDAAC/1504

O’Leary III D S, Kellermann J L, Wayne C (2018). Snowmelt timing, phenology, and growing season length in conifer forests of Crater Lake National Park, USA. Int J Biometeorol, 62(2): 273–285

Ramsay B H (1998). The interactive multisensor snow and ice mapping system. Hydrol Processes, 12(10–11): 1537–1546

Rangwala I, Miller J R (2012). Climate change in mountains: a review of elevation-dependent warming and its possible causes. Clim Change, 114(3–4): 527–547

Riggs G A, Hall D K, Román M O (2017). Overview of NASA’s MODIS and visible infrared imaging radiometer suite (VIIRS) snow-cover earth system data records. Earth Syst Sci Data, 9(2): 765–777

Roth T R, Nolin A W (2017). Forest impacts on snow accumulation and ablation across an elevation gradient in a temperate montane environment. Hydrol Earth Syst Sci, 21(11): 5427–5442

Semmens K A, Ramage J (2012). Investigating correlations between snowmelt and forest fires in a high latitude snowmelt dominated drainage basin. Hydrol Processes, 26(17): 2608–2617

Sherwood J A, Debinski D M, Caragea P C, Germino M J (2017). Effects of experimentally reduced snowpack and passive warming on montane meadow plant phenology and floral resources. Ecosphere, 8(3): e01745

Simic A, Fernandes R, Brown R, Romanov P, Park W (2004). Validation of VEGETATION, MODIS, and GOES + SSM/I snow-cover products over Canada based on surface snow depth observations. Hydrol Processes, 18(6): 1089–1104

Sproles E A, Nolin A W, Rittger K, Painter T H (2013). Climate change impacts on maritime mountain snowpack in the Oregon Cascades. Hydrol Earth Syst Sci, 17(7): 2581–2597

Sproles E A, Roth T R, Nolin A W (2017). A spatial-probabilistic assessment of the extraordinarily low snowpacks of 2014 and 2015 in the Oregon Cascades. Cryosphere, 11(1): 331–341

Steltzer H, Landry C, Painter T H, Anderson J, Ayres E (2009). Biological consequences of earlier snowmelt from desert dust deposition in alpine landscapes. Proc Natl Acad Sci USA, 106(28): 11629–11634

Stewart I T (2009). Changes in snowpack and snowmelt runoff for key mountain regions. Hydrol Processes, 23(1): 78–94

Swenson S C, Lawrence D M (2012). A new fractional snow-covered area parameterization for the Community Land Model and its effect on the surface energy balance. J Geophys Res D Atmospheres, 117 (D21): D21107

Tahir A A, Chevallier P, Arnaud Y, Ahmad B (2011). Snow cover dynamics and hydrological regime of the Hunza River basin, Karakoram Range, Northern Pakistan. Hydrol Earth Syst Sci, 15 (7): 2275–2290

Totland Ø, Alatalo J M (2002). Effects of temperature and date of snowmelt on growth, reproduction, and flowering phenology in the arctic/alpine herb, Ranunculus glacialis. Oecologia, 133(2): 168–175

University of Wyoming (2017). Grand Teton National Park Service Research Needs 2017. http://uwnpsresearch.org/wp-content/uploads/2017/01/Research-Needs-2017GTNP.pdf. Accessed 30 Nov 2017

USGS (2014). Geologic Provinces of the United States: Pacific. http://geomaps.wr.usgs.gov/parks/province/cascade2.html. Accessed 7 Mar 2016

USGS (2017). National Elevation Dataset (NED) The Long Term Archive. https://lta.cr.usgs.gov/NED. Accessed 26 Feb 2017

USGS (2018). United States Geological Survey Current Water Data for the Nation. https://waterdata.usgs.gov/nwis/rt. Accessed 17 Mar 2018

USGSA (2017). Data.gov US General Services Administration. In: Data.gov. https://www.data.gov/. Accessed 26 Feb 2017

Westerling A L, Hidalgo H G, Cayan D R, Swetnam T W (2006). Warming and earlier spring increase western U.S. forest wildfire activity. Science, 313(5789): 940–943

Westerling AL (2016). Increasing western US forest wildfire activity: sensitivity to changes in the timing of spring. Philosophical Transactions of the Royal Society B: Biological Sciences, 371 (1696): 1–10.

Wolf A, Zimmerman N B, Anderegg W R L, Busby P E, Christensen J (2016). Altitudinal shifts of the native and introduced flora of California in the context of 20th-century warming. Glob Ecol Biogeogr, 25(4): 418–429

Yu S, Bhave P V, Dennis R L, Mathur R (2007). Seasonal and regional variations of primary and secondary organic aerosols over the continental United States: semi-empirical estimates and model evaluation. Environ Sci Technol, 41(13): 4690–4697

Zhang X, Friedl M A, Schaaf C B (2006). Global vegetation phenology from moderate resolution imaging spectroradiometer (MODIS): evaluation of global patterns and comparison with in situ measurements. J Geophys Res Biogeosci, 111(G4): G04017

Appendix 1 SNOTEL station validation for the Snowmelt Timing Maps

A1.1 Introduction

Here, we describe in detail the methods and results of the development and validation of the Snowmelt Timing Maps (STMs) for North America 2001–2015 (O'Leary III et al., 2017). These materials are presented here as an Appendix to inform the inquisitive reader of the technical underpinnings of the STMs without distracting from the readability of the primary manuscript.

A1.2 Methods

A1.2.1 Snowmelt timing detection

We developed the STMs (O'Leary III et al., 2017) spanning the area of North America, Greenland, and Iceland using a time-series analysis of the MOD10A2 Collection 5 data product (Hall et al., 2006). The MOD10A2 product is derived from a fractional snow cover product with the snow/no-snow threshold is defined by 50% snow covered area. In this composite product, 8 consecutive days of observations are compiled into a single image representing the 'maximum' snow cover for that period, with each pixel defined as snow-covered if snow was observed for one or more days during the composite period. For example, if a given pixel's 8-day composite period consisted of 4 days of cloud cover, 1 day of snow, and 3 days of bare ground, that pixel would be defined as snow-covered in the composite. This compositing process leads to an 8x reduction in the total number of images for downloading, storage, and processing, and simplifies the cloud interference detection process by removing clouds when possible from the composite images (explained below), though it does represent inferior temporal resolution (8 days rather than 1).

To define snowmelt timing, we record the DOY for the first snow-free image following snow cover, or a mixture of clouds and snow cover (Table 1). For the best-case scenario (Case 1, Table 1), we see two consecutive snow observations preceding one no-snow observation at a given location (pixel). The second-best case (Case 2, Table 1) shows a cloud observation, followed by one snow observation, followed by a no-snow observation at a given location. Early iterations of the STMs did not include Case 2 and had severely degraded quality in mountainous regions where long durations of cloud cover are often followed by a single snow observation before the snow-free period. To manage cloud-obscured MOD10A2 images we interpolated the dates between the last observed snow cover and the first observed snow-free date (Table 1). We recorded cloud interference as the number of consecutive 8-day composite images that were cloud-covered + 1. Pixels with more than four consecutive cloud-obscured images (32 days) between snow and no snow are omitted because of their poor validation results (see validation errors, below). We also calculated the count of STM values ('Count') identifying the number of years on record where the STM has a value (i.e., snow was present at some point that year, and snowmelt timing was successfully calculated).

We obtained the MOD10A2 data from the NSIDC FTP servers in the native HDF4 format and converted to GeoTIFF images using the Geospatial Data Abstraction Library (GDAL.org 2015). Since the MOD10A2 data product record does not begin until DOY 057 (February

26) in the Year 2000, the year 2000 is omitted from our analysis. Each snowmelt timing detection begins on DOY 001 (January 1) and continues through the MOD10A2 image for DOY 249 (September 6) for years 2001–2015. These dates are configured for the Northern Hemisphere where DOY 001 will often already have snow present in seasonal snow zones (Moore et al., 2015), with snow melting during spring and summer through September. Snowmelt occurring after DOY 249 is considered to be outside the scope of the primary snowpack departure identified here. Snowstorms occurring weeks to months after the main snowpack melt are common in North America, and can result in ephemeral snow cover lasting from hours to days (Crawford, 2014).

While late-season snowstorms contribute appreciable water to the ecosystem, they are not the seasonal indicator and hydrologic input of the primary snowpack departure that we seek to capture in the STMs. To remove late-season snowstorms we disregard any snow readings that occur following a 48-day period without snow (six consecutive 8-day composite images) beginning on DOY 57 or later. We chose this 48-day period because it has been shown to be an ecologically significant lag between snowmelt and flowering (Inouye et al., 2002). Additionally, the start date of DOY57 is the 8-day composite date that is closest to March 1, which is often considered to be the beginning of spring for ecological and hydrological investigations that divide the year into four seasons (e.g., March-April-May (MAM) is spring) (Iorio et al., 2004; Yu et al., 2007; Lundquist et al., 2013).

There are three dates in the MOD10A2 dataset with missing data. Year 2001, DOY 169 is missing completely from the NSIDC.org servers. Year 2001, DOY 177 is missing half of the tiles covering North America. In an effort to fill this gap of two successive composite images in the record we took the preceding image (DOY 161) and copied it in place of DOY 169, and took the subsequent image (DOY 185) and copied it in place of DOY 177. For Year 2008, DOY 113 only tile h09v05 is missing, so we copied the subsequent tile (DOY 121) for h09v05 only in place of the missing tile. We then calculated snowmelt timing (described above) using custom python scripts controlling ArcMap 10.3 in the data's native custom Sinusoidal projection. We then calculated a mean snowmelt timing for pixels with at least eight years of coverage and found the 2015 snowmelt anomaly by subtracting the 2015 snowmelt DOY from the 2001–2015 mean snowmelt DOY. For the study areas of the Cascade Mountains and NPS units, we collected NPS boundary and EPA Level III Ecoregion polygons from Data.gov (USGSA, 2017), and elevation data from the USGS National Elevation Dataset (USGS, 2017). There is a small region of CRLA (~25 km^2) that extends outside of the Cascade Mountains polygon (shown in Fig. 1), which is included in the Cascade Mountains region for this study. We then converted all files to a common projection of NAD 1983 UTM 10 N, and resampled the elevation data to match the spatial resolution and registration of the STM using the mean value of the majority sampling technique in ArcMap 10.3.

A1.2.2 Validation

To validate the STMs we compared them with SNOw TELemetry (SNOTEL) stations from across the western United States (NRCS, 2016). Agreement between SNOTEL records and MODIS-based snow products is generally in the range of 80% to 94% (Klein and Barnett, 2003; Brubaker et al., 2005; Hall and Riggs, 2007), though agreement can vary throughout the year (Brubaker et al., 2005) and by land cover type (Hall and Riggs, 2007). To compare the SNOTEL snow water equivalent (SWE) data with the STMs we must derive a snowmelt DOY for each SNOTEL station year (henceforth: SNODOY), which assumes a relationship between SCA and SWE. Parameterizing this relationship is difficult and subject to high uncertainty (Swenson and Lawrence, 2012; Fassnacht et al., 2016), so we assume a SWE of 30 cm to be the snow/no-snow threshold for this comparison, and we discuss the implications of this assumption below. We used an 8-day rolling maximum value window to identify if, at any point in the 8-day window, there was a SNOTEL-reported SWE of greater than 30 cm (mimicking the MOD10A2 snow presence definition). We compared this with an identical 8-day rolling window scanning 8 days later than the previous window. We defined the SNODOY where DOY:DOY + 7 were all below the SWE threshold, and at least one day from DOY-8:DOY-1 were above the SWE threshold. This analysis was performed on a daily time step to match the temporal resolution of the SNOTEL data, which results in a SNODOY where DOY-8 > SWE threshold and DOY: DOY + 7 < SWE threshold.

Comparing the SNODOY with the STMs we must consider the difference in temporal resolution. In the best cases (Table 1, Cases 1,2) the STM DOY value is derived where there is at least one snow-covered day in the preceding 8-day image, and no snow-covered days in the DOY 8-day image. This means that the snowmelt may have occurred any time during the preceding 8-day composite image, because a single day of snow presence any time in the 8-day period is shown as snow in the MOD10A2 image. By comparison, the SNODOY is calculated daily, therefore the transition from SWE > 30 cm to SWE = < 30 cm always occurs from DOY-8 to DOY-7. In this way the SNODOY always reports the DOY 8 days after the actual transition that we identify, whereas the STMs may indicate DOY anywhere from 1 to 8 days after the actual snowmelt (Table A1), therefore the STM-SNODOY may have a discrepancy ranging from 0 to –7 days. For example, consider a theoretical persistent snowpack that is deep and widespread, such that it was identified in both the STM and SNOTEL datasets. If this snow were to melt rapidly on DOY 135, that transition

would be identified as DOY 143 using the SNODOY method, however the next 8-day composite MOD10A2 map is DOY 137, therefore the STM would mark that snowmelt as DOY137, resulting in a difference of –6 days. Assuming a random distribution of detection errors from 0 to –7 days, we offset our resulting errors by + 3.5 days resulting in the equation Error = STM – SNODOY + 3.5 days. For this validation, we first used all SNOTEL locations for their available period of record, including stations outside our study area, discarding any SNOTEL station that had zero snow according to either SNODOY or STMs. We then calculated errors between the SNOTEL stations and the STM by subtracting the SNOTEL snowmelt DOY from the STM snowmelt DOY, and adding 3.5 as described above. Next, we subset the SNOTEL locations selecting only those within the Cascade Mountains EPA Level III ecological region to identify SNOTEL/STM agreement for our area of interest. We calculated the mean and standard deviation of the errors for the full SNOTEL record ($n = 854$), and the Cascade Mountains stations ($n = 65$). We tested the distributions of errors for normality using the Shapiro-Wilk test ($\alpha = 0.10$). The full SNOTEL error record is larger than 5000, violating the assumption of the Shapiro-Wilk test ($n <= 5000$), therefore we randomly sampled 1000 values without replacement and tested for normality, and repeated this ten times.

Table A1 Examples of the differences in the STM and SNODOY results. In ideal, clear sky conditions the STM reports snowmelt within 8-day ranges (001, 009, 017, 025, etc.), whereas the SNOTEL stations allow for a daily time step

Last day of snow presence	STM	SNODOY
DOY = 001	009	009
DOY = 005	009	013
DOY = 008	009	016
DOY = 009	017	017

A1.3 Results

Validation results between the STMs and SNOTEL stations ($n = 854$) reveals a high level of agreement (Fig. A1). With the exception of 2004, all annual mean errors are non-normally distributed ($\alpha = 0.10$) with means ranging from −0.81 (2008) to 7.40 (2015). Analysis of the SNOTEL stations within the Cascade Mountains Eco-region ($n = 65$) show a fair agreement between the STMs and SNODOY (Fig. A2) with nine of the fifteen years on record showing normally distributed errors ($\alpha = 0.10$). Year 2015 in the Cascade Mountains region had a poor comparison between the STM and the SNODOY because only seven SNOTEL stations had SWE values that exceeded 30 cm during the 2015 period of analysis. When we compile all errors for all years, both the full SNOTEL and the Cascade Mountains SNOTEL subset show strong agreement with the STMs (Fig. A3). Errors between the STMs and the full SNOTEL record have a mean of 4.31, standard deviation of 17.52, skewness of 0.39, and kurtosis of 5.36. Errors between the Cascade Mountains SNOTEL subset and the STMs have a mean of −4.76, standard deviation of 21.70, skewness of 0.98, and kurtosis of 7.75. While neither sample is normally distributed ($\alpha = 0.10$), both have a low skewness, showing that errors are mostly symmetrical about the mean, and high kurtosis, showing that most errors are close to the mean. Both samples have distant outliers, which are likely caused when the STMs identify a snow event of >50% SCA that is less than 30 cm SWE at the SNOTEL station (or vice versa). The slight positive skew for both samples indicates that it is more likely for these mis-matches to occur when the STMs identify snow cover that is insufficient to meet the SNOTEL snow-presence threshold of 30 cm. Cloud interference increases the error between the STM and SNODOY, as greater cloud interference values lead to increasingly negative errors (Table A2, Fig. A3).

A1.4 Discussion

Comparison of the STMs and SNOTEL shows generally strong agreement. The variability of the errors emphasizes the patchy nature of a snowpack, especially during snowmelt. Snow patches, even when covering more than 50% of the land surface at the MODIS resolution (resulting in a "snow" reading for the MOD10A2 product), may retain little to no SWE at the SNOTEL station. It is likely that the spatial heterogeneity of snow below the 500 m MODIS resolution leads to frequent disagreement between the STM and SNOTEL snowmelt values (Fassnacht et al., 2016). When combining all years, the average disagreement between the STMs and SNODOY is 4.31days and –4.76 days for all SNOTEL and just the Cascade Mountains stations, respectively. These errors are fairly small relative to the temporal resolution of the MOD10A2 product (8 days), though the wide distribution of errors indicates that there is still much variability on the ground. In comparing the STMs and SNOTEL stations we assumed a SWE value of 30 cm at the SNOTEL station equals 50% SCA from the MODIS product. In locations where this value is a poor fit, systematic disagreements may be present, though the overall distribution of errors shows that these two data sources may be favourably compared. The Cascade Mountains show an earlier melt according to the SNOTEL station compared to the STM, perhaps indicating that in the Cascade Mountains a higher SWE corresponds to 50% SCA than compared with other regions. This bias may be improved by optimizing the snowmelt SWE threshold by ecoregion or particular area of interest. Our

findings support other work focusing on the difficulties in comparing snow data of varying spatial resolutions and measurement methods (Klein and Barnett, 2003; Brown et al., 2003; Simic et al., 2004; Brubaker et al., 2005).

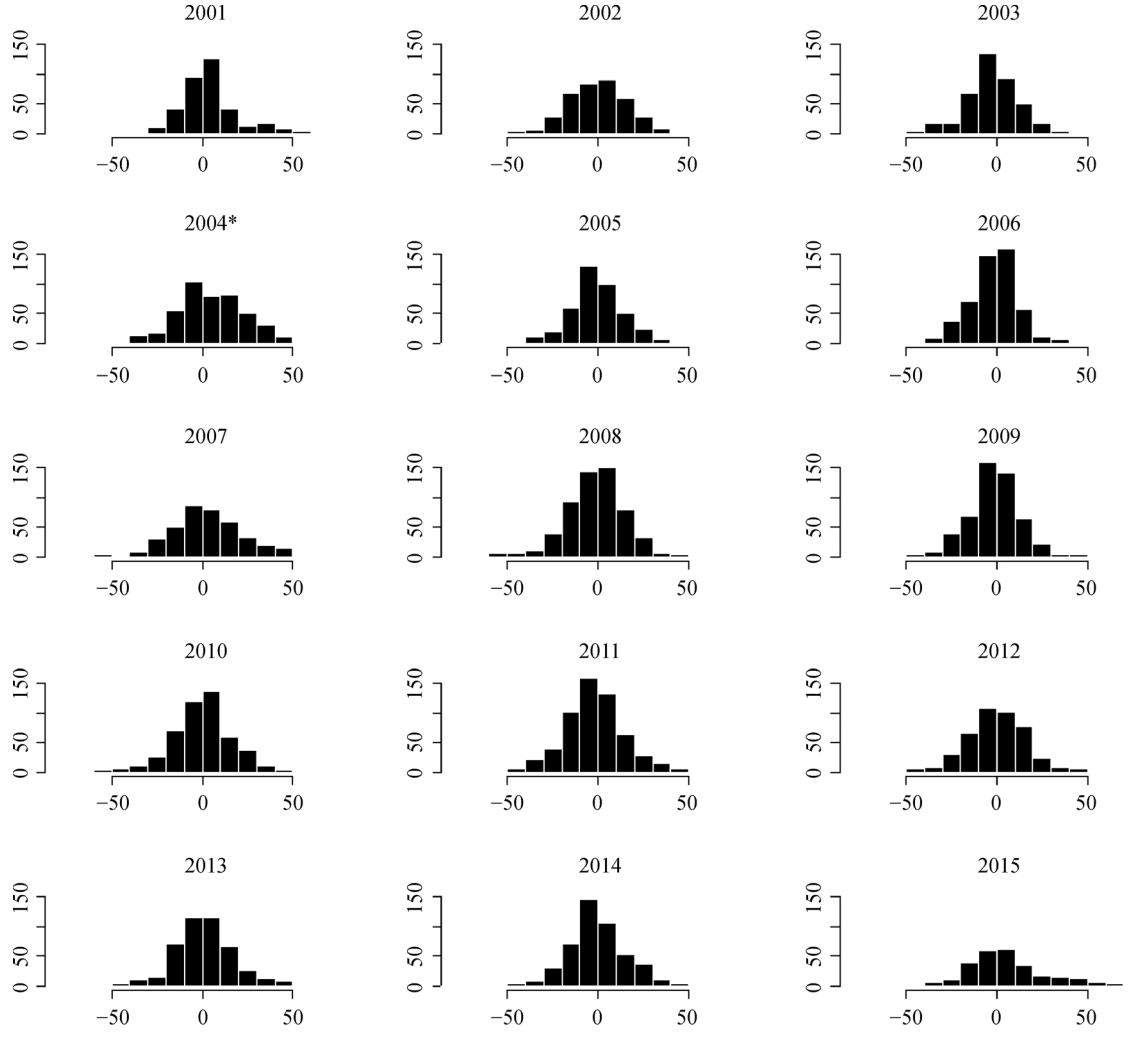

Fig. A1 Histograms illustrating the errors between the Snowmelt Timing Maps (STMs) and SNOTEL stations (days, *x* axis; frequency, *y*-axis). Errors are calculated by subtracting the SNOTEL melt Day Of Year (SNODOY) from the STM DOY. Errors are non-normally distributed ($\alpha = 0.10$) about means ranging from 0.81 (2008) to 7.40 (2015), except for 2004, which is normally distributed.

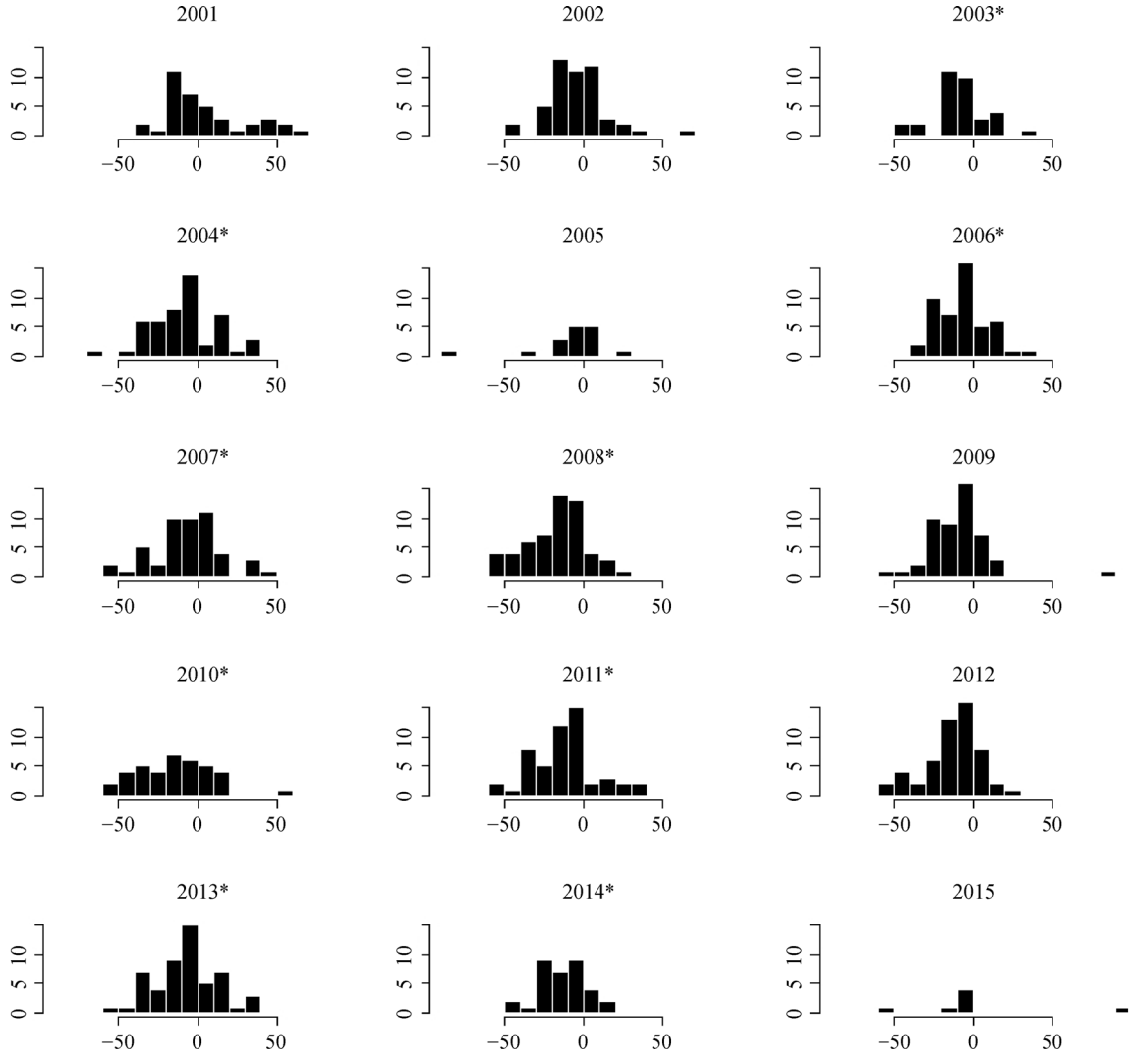

Fig. A2 Histograms describing the errors between the Snowmelt Timing Maps (STMs) and SNOTEL stations (days, *x* axis; frequency, *y*-axis) for all SNOTEL locations within the Cascade Mountains Ecoregion for years 2001–2015. Years marked with an asterisk are normally distributed ($\alpha = 0.10$). Means range from 17.05 (2008) to + 5.03 (2001).

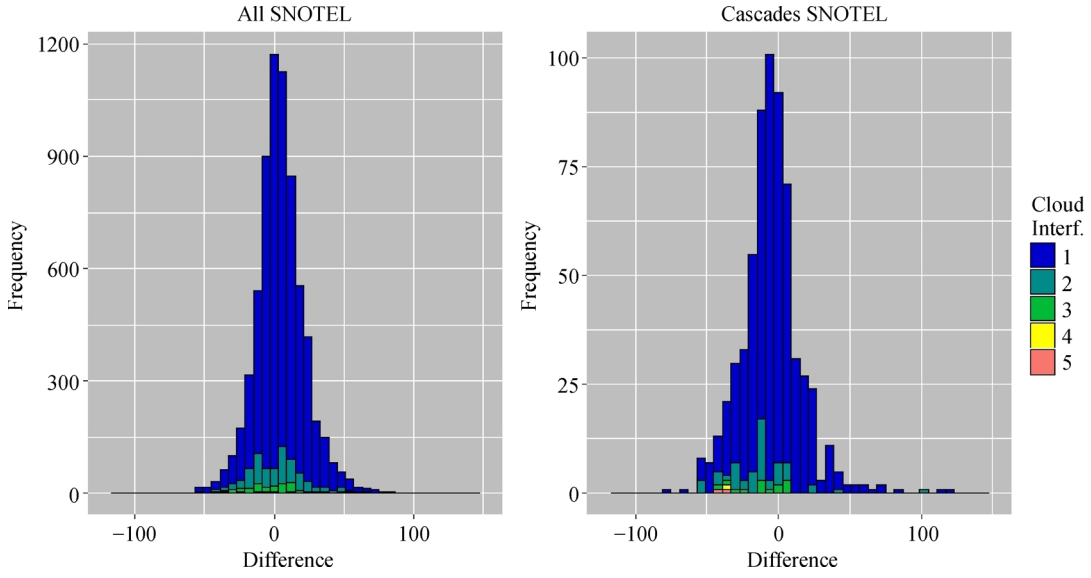

Fig. A3 Histograms of errors between the Snowmelt Timing Maps (STMs) and SNOTEL stations (days, *x* axis; frequency, *y*-axis) for the entire period of record for all SNOTEL sites, and those within the Cascade Mountains Ecoregion, calculated as STM-SNODOY + 3.5. Colors indicate cloud interference value (1 = no cloud interference, 5 = four consecutive 8-day composite images of clouds). Both populations are centered about means of 4.31 and –4.76 with standard deviations of 17.53 and 21.70, respectively. Clouds interfered with 10.67% of readings for all SNOTEL stations, and 11.92% of those within the Cascade Mountains Ecoregion.

Table A2 Description of the population of validation errors by cloud interference value

CI value	All SNOTEL stations			Cascade Mountains only		
	n	% of total	Mean/days	*n*	% of total	Mean/days
All	8736	100%	4.31	671	100%	–4.76
1	7804	89.33%	4.69	591	88.08%	–3.75
2	735	8.41%	1.96	61	9.09%	–12.23
3	162	1.85%	0.35	16	2.38%	–12.88
4	28	0.32%	–3.24	1	0.15%	–36.5
5	7	0.08%	–11.67	2	0.30%	–40